Human Molecular Genetics, 2020, Vol. 29, No. 15 2596–2610

doi: 10.1093/hmg/ddaa152
Advance Access Publication Date: 18 July 2020
General Article

GENERAL ARTICLE

Ubiquilin-2 differentially regulates polyglutamine disease proteins

Julia E. Gerson, Nathaniel Safren, Svetlana Fischer, Ronak Patel, Emily V. Crowley, Jacqueline P. Welday, Alexandra K. Windle, Sami Barmada, Henry L. Paulson* and Lisa M. Sharkey*

Department of Neurology, University of Michigan, Ann Arbor, MI 48109-2200, USA

*To whom correspondence should be addressed. Henry L. Paulson, Tel: (734) 615-5632; Fax: (734) 647-9777; Email: henryp@umich.edu; Lisa M. Sharkey, Tel: (734) 763-3496; Fax: (734) 647-9777; Email: lisams@umich.edu

Abstract

Divergent protein context helps explain why polyglutamine expansion diseases differ clinically and pathologically. This heterogeneity may also extend to how polyglutamine disease proteins are handled by cellular pathways of proteostasis. Studies suggest, for example, that the ubiquitin-proteasome shuttle protein Ubiquilin-2 (UBQLN2) selectively interacts with specific polyglutamine disease proteins. Here we employ cellular models, primary neurons and mouse models to investigate the potential differential regulation by UBQLN2 of two polyglutamine disease proteins, huntingtin (HTT) and ataxin-3 (ATXN3). In cells, overexpressed UBQLN2 selectively lowered levels of full-length pathogenic HTT but not of HTT exon 1 fragment or full-length ATXN3. Consistent with these results, UBQLN2 specifically reduced accumulation of aggregated mutant HTT but not mutant ATXN3 in mouse models of Huntington's disease (HD) and spinocerebellar ataxia type 3 (SCA3), respectively. Normally a cytoplasmic protein, UBQLN2 translocated to the nuclei of neurons in HD mice but not in SCA3 mice. Remarkably, instead of reducing the accumulation of nuclear mutant ATXN3, UBQLN2 induced an accumulation of cytoplasmic ATXN3 aggregates in neurons of SCA3 mice. Together these results reveal a selective action of UBQLN2 toward polyglutamine disease proteins, indicating that polyglutamine expansion alone is insufficient to promote UBQLN2-mediated clearance of this class of disease proteins. Additional factors, including nuclear translocation of UBQLN2, may facilitate its action to clear intranuclear, aggregated disease proteins like HTT.

Introduction

The disease proteins implicated in polyglutamine expansion disorders differ widely in structure and function. This divergent protein context probably accounts for much of the clinical and neuropathological differences across this class of neurodegenerative diseases. An important factor contributing to disease differences and potential disease-specific therapeutic targets is the differential interaction between distinct polyglutamine proteins and various components of protein homeostatic pathways. The ubiquitin-dependent protein clearance factor Ubiquilin-2 (UBQLN2), which has recently been implicated in numerous neurodegenerative diseases (1,2), offers insight into the dysfunction of protein quality control pathways in disease. UBQLN2 is one member of a family of brain-expressed ubiquilins that also includes UBQLN1 and UBQLN4. All ubiquilins possess N-terminal ubiquitin-like (UBL) and C-terminal ubiquitin-associated (UBA) domains, which together enable ubiquilins to shuttle ubiquitinated proteins to the proteasome for degradation (3,4). UBQLN2 principally functions in proteasomal clearance of ubiquitinated substrates, but also modulates autophagic clearance of aggregates (5) and may serve other roles in protein quality control (6–8).

Received: March 13, 2020. **Revised:** July 7, 2020. **Accepted:** July 13, 2020

Although evidence suggests the primary function of UBQLN2 is to promote protein homeostasis by facilitating the clearance of misfolded and aggregating proteins, UBQLN2 itself shares with many other neurodegenerative disease proteins the propensity to undergo liquid–liquid phase separation and form aggregates *in vitro* (9,10). The fact that missense mutations in UBQLN2 directly cause frontotemporal dementia (FTD) and amyotrophic lateral sclerosis (ALS) (2,11–13) underscores the importance of this family of proteins in neurodegenerative proteinopathies. The dynamics of UBQLN2 function as a clearance factor for disease proteins on the one hand, and its potential dysfunction and toxicity under various disease conditions on the other hand, are poorly understood.

We and others have shown that UBQLN1 and UBQLN2 colocalize with aggregates of mutant huntingtin (HTT) in mouse models of Huntington's disease (HD) and tissue from human HD patients, but not with aggregates of ataxin-3 (ATXN3) in spinocerebellar ataxia type 3 (SCA3) (1,14–16). Although both ATXN3 and HTT are polyglutamine disease proteins that, when harboring an expansion, redistribute to the nucleus and form intranuclear inclusions of aggregated protein, UBQLN2 appears to selectively bind HTT and not ATXN3. UBQLN2 depletion can increase aggregated mutant HTT in cellular and animal models (17), but despite studies suggesting UBQLN2 interacts with HTT (1,14–16), it is not known whether UBQLN2 expression conversely decreases mutant HTT or other polyglutamine disease proteins, such as ATXN3. Questions also remain concerning which factors contribute to UBQLN2 substrate selectivity and whether substrate binding is inextricably linked to substrate clearance.

To better understand the selective regulation of polyglutamine proteins by UBQLN2, we used cellular and transgenic mouse models of HD or SCA3 to investigate UBQLN2-dependent regulation of polyglutamine disease proteins and modulation of pathology *in vivo*. Notably, in neurodegenerative diseases associated with polyglutamine expansion including SCA3 and HD, protein aggregates primarily accumulate in the nucleus (18), whereas ATXN3 and HTT are normally cytoplasmic proteins (19,20). Accordingly, we also assayed for changes in subcellular localization of UBQLN2, which is thought to be largely a cytoplasmic protein, when mutant HTT or ATXN3 is present. Our results show that UBQLN2 differentially reduces polyglutamine substrates and suggest that cellular localization of UBQLN2 influences its ability to regulate specific intranuclear disease aggregates. Our data further suggest that even though UBQLN2 normally participates in quality control pathways, increasing UBQLN2 levels actually can enhance the accumulation of some disease-linked proteins, highlighting the need to better understand the mechanisms underlying UBQLN2 function, subcellular localization and aggregation.

Results

UBQLN2 decreases levels of full-length HTT, but not of HTT exon 1 fragment or ATXN3

The fact that UBQLN2 is a proteasome shuttle protein which accumulates in various neurodegenerative diseases suggests that it may broadly regulate levels of misprocessed disease proteins. To evaluate UBQLN2's ability to lower levels of polyglutamine disease proteins, we transiently expressed or knocked down UBQLN2 in HEK-293 cells while also expressing two different polyglutamine disease proteins, the HD protein HTT and the SCA3 protein ATXN3. Assessed by western blot, co-expressed UBQLN2 significantly decreased both wildtype and polyglutamine-expanded full-length HTT levels (wildtype: $P = 0.01$; expanded: $P = 0.01$; Fig. 1A). Knockdown of UBQLN2 did not lead to an increase of HTT (wildtype: $P = 0.85$; expanded: $P = 0.99$; Fig. 1A).

In contrast, levels of a polyglutamine-expanded N-terminal HTT exon 1 fragment (comprising ~3% of the full-length protein and commonly used to study aggregation of polyQ-expanded HTT) were not robustly affected by UBQLN2 overexpression (wildtype: $P = 0.99$; expanded: $P = 0.13$) or siRNA knockdown (wildtype: $P = 0.13$; expanded: $P = 0.97$; Fig. 1B). Levels of a second polyglutamine protein, ATXN3, also were not robustly changed by UBQLN2 expression (wildtype ATXN3: $P = 0.79$; expanded ATXN3: $P = 0.23$) or knockdown (wildtype ATXN3: $P = 0.78$; expanded ATXN3: $P = 0.33$; Fig. 1C). To confirm that UBQLN2 does not simply down-regulate any overexpressed protein, we assessed the effect of UBQLN2 on the reporter protein, GFP. Levels of GFP were unchanged by modulating UBQLN2 (overexpression: $P = 0.44$; knockdown: $P = 0.79$; Fig. 1D). Measurement of UBQLN2 levels (normalized to empty vector control) in cells transfected with UBQLN2 plasmid or UBQLN2 siRNA demonstrated that cotransfection with HTT or ATXN3 plasmids did not alter the degree of UBQLN2 overexpression or knockdown (overexpression: $P = 0.97$; knockdown: $P = 0.99$; Fig. 1E). The differing ability of UBQLN2 to alter levels of HTT versus ATXN3 is consistent with our earlier report that UBQLN2 interacts with and localizes to inclusions of HTT but not of ATXN3 in murine disease models and human disease brain (14). This differential effect suggests UBQLN2 does not simply regulate any overexpressed or aggregate-prone protein containing expanded polyglutamine.

UBQLN2 overexpression in neurons does not reduce toxicity or inclusions derived from expanded HTT exon 1 fragment

To further probe the ability of UBQLN2 to regulate toxicity from a polyglutamine expansion in a disease-relevant cell type, we used automated fluorescence microscopy (AFM) (21) to assess the survival of rat cortical neurons co-expressing iRFP-UBQLN2 and either GFP-HTT-exon1-wildtype (Q17) or mutant (Q72) (hereafter called HTT fragment) (Fig. 2A). Survival data from these experiments were assessed using Cox proportional hazards analysis, a time-to-event statistical model frequently used in clinical trials to compare the cumulative risk of cell death for each neuronal population. This method enables us to calculate a hazard ratio for each condition, representing the relative risk of death compared to the reference or control group, allowing direct comparisons of toxicity between and among conditions.

Relative to neurons expressing wildtype (Q17) HTT fragment, the hazard ratio of neurons expressing mutant (Q72) HTT fragment was 1.5, signifying that these neurons died 50% faster (Fig. 2B) (Supplementary Material, Table S1, Cox proportional hazards, $P = 5.4 \times 10^{-23}$). In accordance with our previous work (9), UBQLN2 overexpression alone enhanced the risk of death by roughly 20% (Supplementary Material, Table S1, Cox proportional hazards, hazard ratio = 1.22, $P = 1.19 \times 10^{-5}$). UBQLN2 did not alter toxicity from HTT fragment overexpression, as neurons co-expressing GFP-HTT-exon1-Q72 and iRFP-UBQLN2 died at comparable rates to those expressing GFP-HTT-exon1-Q72 and the iRFP control (Supplementary Material, Table S1, Cox proportional hazards, hazard ratio = 1.04, $P = 0.41$).

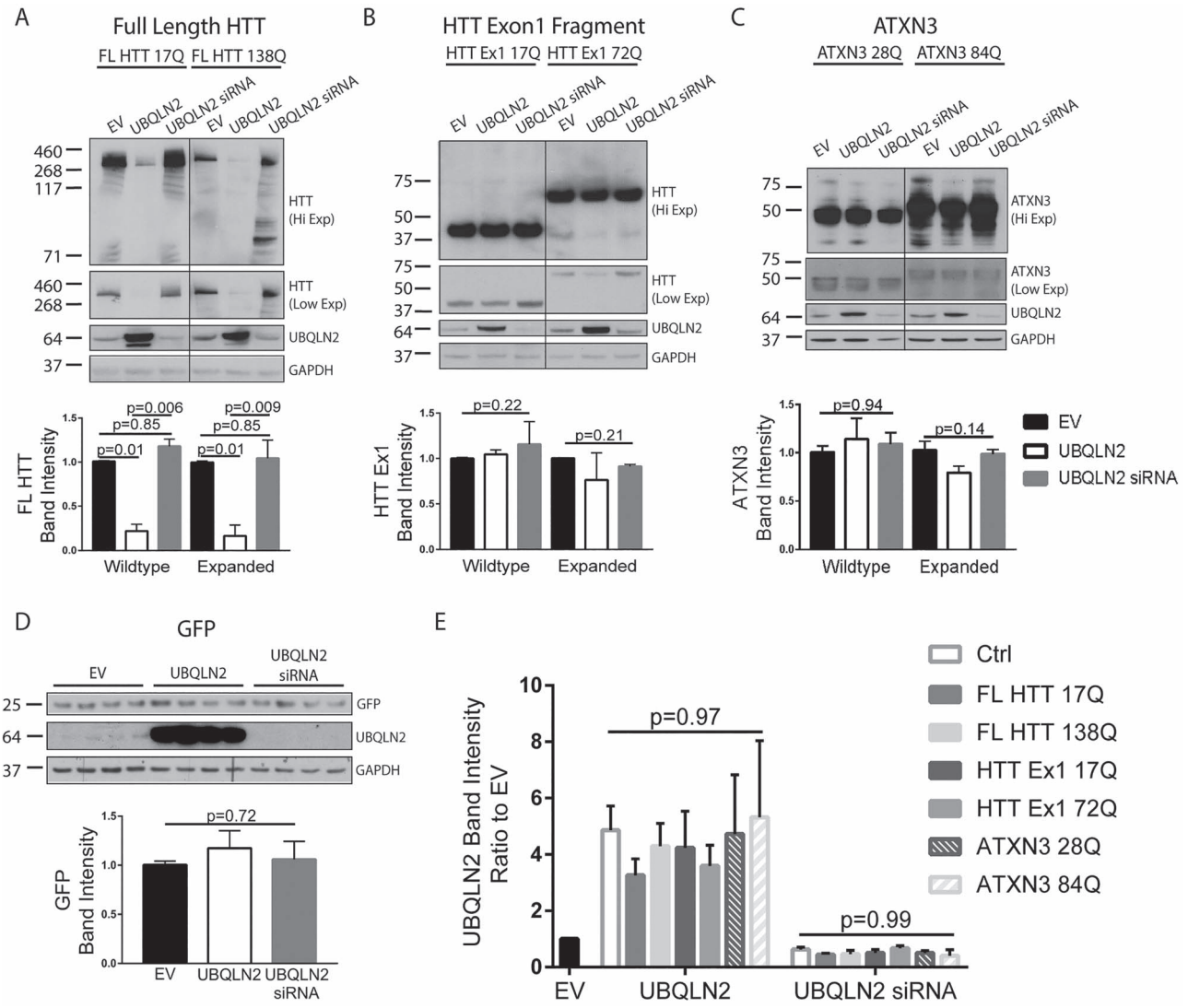

Figure 1. UBQLN2 regulates levels of full-length HTT, but not other tested polyglutamine proteins, in HEK-293 cells. (**A**) Full-length HTT is significantly decreased by UBQLN2 expression ($n = 6$), (**B**) whereas HTT exon 1 fragment is unaffected ($n = 6$). (**C**) Levels of the SCA3 disease protein, ATXN3 (normal or expanded), are not significantly altered by UBQLN2 expression or knockdown ($n = 8$). (**D**) Levels of reporter protein GFP are unchanged by UBQLN2 expression or knockdown ($n = 6$). (**E**) Co-expression of HTT or ATXN3 plasmids does not alter levels of UBQLN2 overexpression and knockdown. All band density quantifications (averaged across all technical replicates) were carried out on low exposure (Low Exp) blots normalized to GAPDH and to empty vector control for each experiment to allow for comparison between technical replicates; high exposures (Hi Exp) are shown for qualitative visualization of high molecular weight species and protein fragments. P-values for overall ANOVAs are displayed in analyses that did not show a significant difference, whereas individual post-hoc comparison P-values are displayed for significant ANOVAs.

Previously, we established the coefficient of variation (CV) as a sensitive and specific measure of protein aggregation in neurons expressing fluorescently tagged proteins (9). The aggregation of these proteins into puncta produces distinct peaks in fluorescence intensity, increasing the standard deviation of fluorescence intensity integrated over the cell area ($SD_{intensity}$). Indeed, $SD_{intensity}$ by itself has been successfully used to identify neurons with and without fluorescent puncta (22). Here, we took into account single-cell variations in expression by scaling all calculations of $SD_{intensity}$ by the mean fluorescence intensity and generating a CV for each cell. We leveraged this approach to quantify HTT fragment inclusions in a high-throughput and unbiased way. In a test dataset of 500 neurons, HTT-Q72-GFP CV successfully predicted the presence of inclusions with high selectivity [2% false-positive (FP) rate] and sensitivity [92% true-positive (TP) rate] (Fig. 2C).

We used this method of single-cell CV measurements to assess the percentage of living neurons containing HTT fragment inclusions over the span of 8 days. In accordance with previous studies (15,17), showing a direct interaction between UBQLN2 and mutant HTT fragment, we found that UBQLN2 and HTT-exon1-Q72 colocalized to inclusions in neurons (Fig. 2E). However, supporting our results in HEK-293 cells, co-expression of UBQLN2 with Q72 HTT fragment had no effect on the percentage of neurons containing HTT inclusions (Fig. 2D), suggesting that interaction with UBQLN2 does not affect mutant HTT fragment levels or aggregation.

UBQLN2 overexpression reduces HTT pathology *in vivo*

Because HTT is such a large protein, it is technically difficult to extend the above neuronal studies to the full-length disease

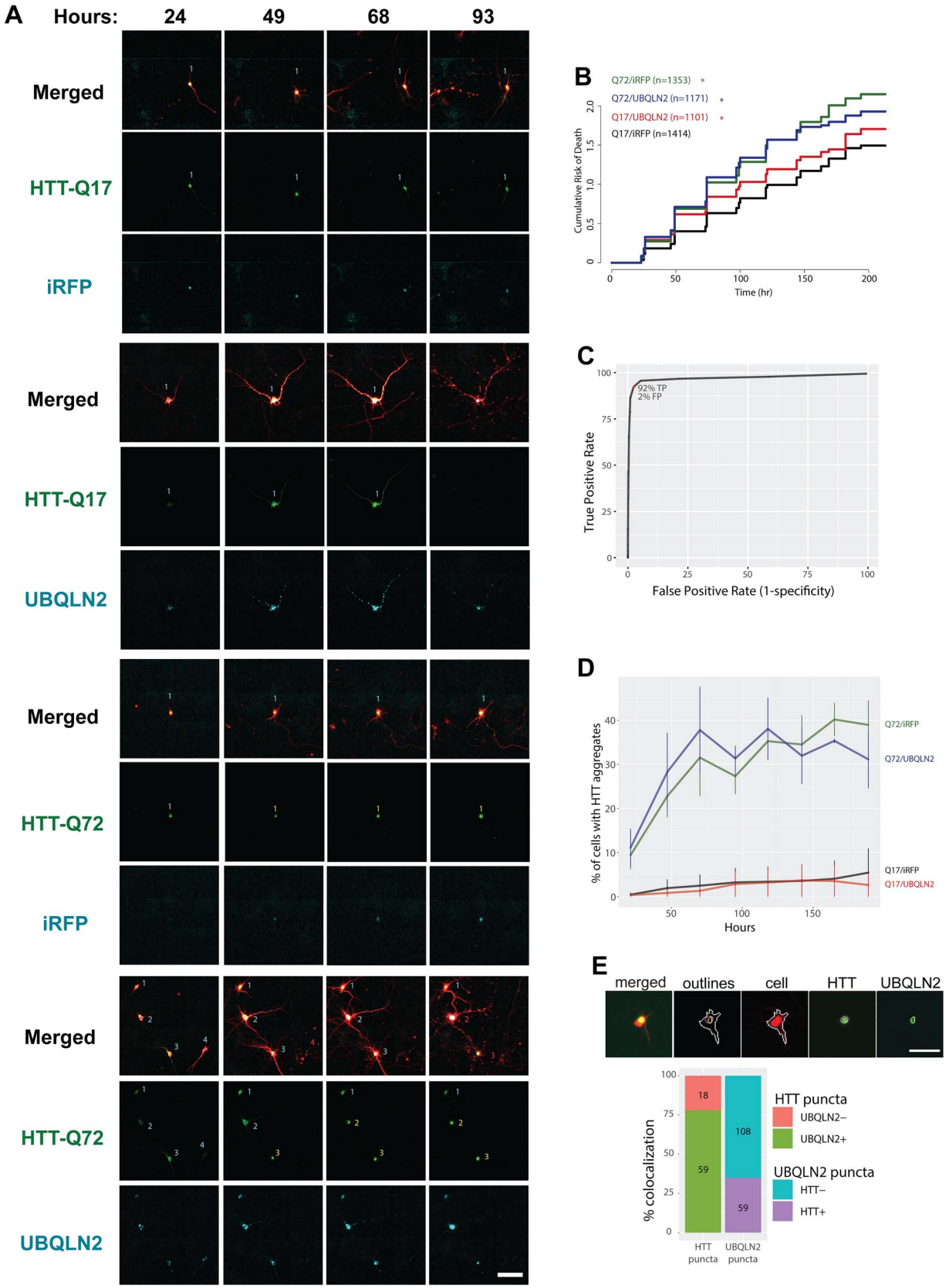

Figure 2. UBQLN2 expression does not enhance the clearance of exon 1 mutant HTT fragment in primary cortical neurons. (**A**) E20 primary rat cortical neurons co-transfected on DIV 4 with GFP-Exon1-HTT-Q17 or GFP-Exon1-HTT-Q72 (green), iRFP or iRFP-UBQLN2 (cyan) and mApple (red). Neurons were assigned unique identifiers (numbers adjacent to cells) and longitudinally imaged by AFM. For each neuron the time of cell death (dead cells denoted with red numbers in 'merged' rows) and HTT puncta formation (HTT puncta denoted with yellow numbers in 'HTT' rows) were recorded. Scale bar = 100 μm. (**B**) Cumulative risk of death plot illustrating that

protein. Accordingly, we employed genetic crosses *in vivo* to test whether our results in cellular models extended to HD and SCA3 models expressing the full-length disease proteins. We crossed UBQLN2 transgenic mice to the HD200 knock-in mouse model of HD, which expresses HTT with a hyperexpansion of ~200 repeats (Fig. 3A) (23,24). Mutant HTT levels in whole brain lysate were significantly reduced by UBQLN2 co-expression, while endogenous levels of non-pathogenic HTT were unchanged (Fig. 3B). HD200 mice are known to develop prominent intranuclear HTT inclusions by 6–8 months of age (23). Co-expression of UBQLN2 markedly decreased HTT intranuclear inclusions throughout the brain, with the greatest effect seen in the hippocampus (Fig. 3C and D). These results are consistent with our earlier cellular results showing a UBQLN2-driven decrease in total levels of full-length HTT and confirm our hypothesis that UBQLN2 robustly counters accumulation of full-length mutant HTT, possibly through ubiquitin-dependent protein degradation based on the known roles of UBQLN2.

Intriguingly, UBQLN2 is principally a cytoplasmic protein in neurons yet when co-expressed with mutant HTT, UBQLN2 translocated to the nuclei of neurons. This subcellular redistribution of UBQLN2 was most notable in the hippocampus, the region in which we saw the most robust HTT reduction by UBQLN2 (Fig. 4A, C and D). Overexpressed UBQLN2 often co-localized with the few remaining mutant HTT inclusions in HD200/UBQLN2 mouse brain (Fig. 4E-H).

UBQLN2 overexpression fails to decrease ATXN3 accumulation *in vivo*

In contrast to results in the HD mouse model, UBQLN2 overexpression in a cross to a SCA3 mouse model (Fig. 5A) did not alter levels of ATXN3 in whole brain homogenate (Fig. 5B-D). For this cross, we used the YAC SCA3 (SCA3-84) mouse model that expresses the full human disease gene with a CAG expansion of 84 repeats (25,26). Pathogenic accumulation of ATXN3 in the nuclei of affected brain regions is the hallmark of disease in human patients and the SCA3-84 mouse model. We measured the degree of ATXN3 nuclear accumulation by quantifying the co-localization of ATXN3 signal with DAPI signal in immunofluorescently stained tissue sections. ATXN3 nuclear levels in a particularly vulnerable neuronal population in SCA3, the deep cerebellar nuclei (DCN), were unaffected by UBQLN2 expression, while levels were only modestly decreased in the pons (Fig. 5E, H). UBQLN2 rarely colocalized with nuclear ATXN3 (Fig. 5F, I). UBQLN2 also failed to redistribute to neuronal nuclei in the SCA3 model (Figs 5G, J; 6D, H), in contrast to what we observed in the HD200 cross. UBQLN2 co-expression also had no effect on the number of nuclear ATXN3 puncta in cortical neurons (Fig. 6A). Remarkably, UBQLN2 overexpression led to an accumulation of cytoplasmic ATXN3 puncta in both cortical and hippocampal neurons, which is not normally seen in SCA3-84 mice (Fig. 6A, E). These ATXN3 puncta were largely negative for co-staining of UBQLN2 (Fig. 6B-C, F-G).

Discussion

UBQLN2 is implicated in various neurodegenerative diseases, but its ability to regulate a range of disease proteins has not been systematically evaluated. Collectively our results support the ability of UBQLN2 to regulate, in a selective manner, polyglutamine disease proteins, presumably by facilitating protein clearance. Our findings are consistent with previous studies identifying HTT as a substrate for UBQLN2-mediated degradation (17) and studies showing that UBQLN2 localizes to disease aggregates in HD brain (14,15,17). Our results with additional polyglutamine substrates, in particular the SCA3 disease protein ATXN3, support the view that UBQLN2 action toward polyglutamine substrates varies greatly, based on protein context.

While UBQLN2 has been shown to bind mutant HTT fragments in both cellular and animal models (5,15,17), we find that the HTT exon 1 fragment is not readily handled by UBQLN2. Unlike ATXN3, which does not interact with UBQLN2, HTT fragment appears not to be a substrate for UBQLN2 despite binding it, suggesting that interaction with and clearance by UBQLN2 are not inextricably linked. While our results establish that UBQLN2 decreases full-length mutant HTT, the precise mechanism of action remains uncertain. Based on well-documented interactions between ubiquilins and HTT (5,17,27), we suspect that UBQLN2 regulates HTT at the level of ubiquitin-dependent proteasomal clearance rather than at the transcriptional or translational level.

Our data suggest UBQLN2 recruitment to the nucleus is relevant to its mechanism of action, given that in neurons of HD mice, the normally cytoplasmic UBQLN2 redistributes to the nucleus, the subcellular site where HTT inclusions accumulate. In the setting of UBQLN2 overexpression, the few remaining intranuclear HTT inclusions are largely positive for UBQLN2, further highlighting the potential importance of UBQLN2 localization to the nucleus for the regulation of HTT (Fig. 4). By contrast, UBQLN2 does not redistribute to the nucleus of neurons in SCA3 mice even though the nucleus is the subcellular site where mutant ATXN3 accumulates and aggregates. These results suggest nuclear localization of UBQLN2 facilitates its ability to decrease pathological intranuclear proteins.

Nevertheless, it is still unclear whether UBQLN2 acts to reduce HTT accumulation in the cytoplasm or nucleus. Conceivably, mutant HTT recruits UBQLN2 to the nucleus as part of a surveillance mechanism, given the potential importance of DNA damage in HD (28). While proteasomal clearance primarily

UBQLN2 expression had no effect on the rate of cell death in neurons expressing GFP-exon1-HTT-Q72 (hazard ratio 1.04, $P = 0.41$ Cox proportional hazards analysis). Neurons in each group were pooled from three replicate experiments and experiment date was used for stratification in cox proportional hazards analysis. Asterisk denotes significant difference from Q17/iRFP ($P < 0.05$, Cox proportional hazard). Hazard ratios and significance values are reported in Supplementary Material, Table S1. (**C**) Receiver operating characteristic curve illustrating the sensitivity (TP rate = 92%) and specificity (FP rate = 2%) of GFP-exon1-HTT-Q72 CV for detecting puncta formation in individual neurons. (**D**) Percentage of living neurons containing HTT puncta at each time point. Beginning 48 h after transfection, neurons expressing GFP-exon1-HTT-Q72 displayed significantly more puncta than neurons expressing GFP-exon1-HTT-Q17. At no point did co-expression of UBQLN2 have any effect on the percentage of cells with GFP-exon1-HTT-Q72 puncta (two-way ANOVA with repeated measures, Tukey's multiple comparisons test significance: $P < 0.05$). Error bars represent standard error of the mean from three replicate experiments. (**E**) A subset of HTT and UBQLN2 inclusions colocalize in neurons (top panel). Cell body (red/white outline), HTT inclusion (green/magenta outline) and UBQLN2 inclusion (cyan/yellow outline) regions of interest were generated in an unbiased manner using CellProfiler (bottom left panel). In neurons containing both HTT and UBQLN2 inclusions ($n = 61$ neurons), each HTT punctum was classified as either colocalizing with UBQLN2 inclusions (UBQLN2+ HTT puncta, $n = 59$) or not colocalizing with UBQLN2 inclusions (UBQLN2- HTT puncta, $n = 18$). Conversely, each UBQLN2 inclusion was classified as either colocalizing with HTT puncta (HTT+ UBQLN2 puncta, $n = 59$) or not colocalizing with HTT puncta (HTT-UBQLN2 puncta, $n = 108$). Normalized data represent each fraction as a percentage of all inclusions (bottom right panel). Scale bar = 50 μm.

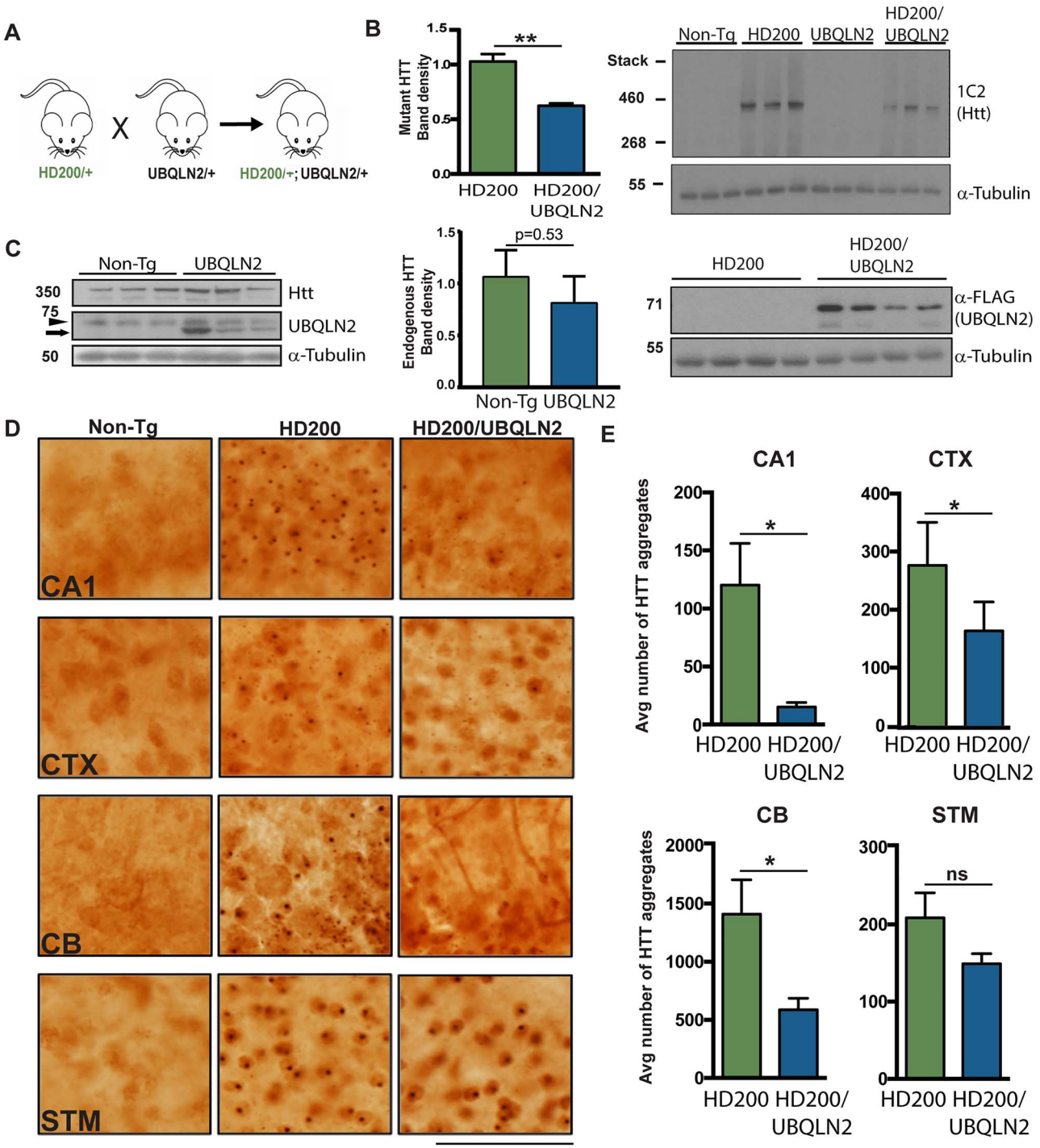

Figure 3. UBQLN2 reduces mutant HTT levels and aggregation in a knock-in mouse model of HD. (**A**) Breeding strategy to produce HD knock-in mice (HD200) expressing mutant HTT alone or with overexpressed WT- UBQLN2. (**B**) Left: quantification of expanded endogenous HTT levels detected by western blot and normalized to α-tubulin ($n = 9$ mice per genotype). Right: representative western blot of whole brain lysates probed with the anti-polyglutamine 1C2 antibody to detect mutant HTT and FLAG antibody to detect transgenic UBQLN2. Lysates from three mice of each genotype are shown for HTT and four mice of each genotype for UBQLN2. Significant differences in mutant (expanded) HTT between HD200 mice and HD200/UBQLN2 mice were identified with an unpaired *t*-test. $^{**}P \leq 0.01$. 'Stack' marks the bottom of the stacking gel. (**C**) Left: representative western blot of whole brain lysates probed with the anti-HTT clone 1HU-4C8 antibody for endogenous murine HTT and UBQLN2 antibody (arrowhead labels endogenous murine UBQLN2 while arrow labels transgenic human UBQLN2). Lysates from three mice of each genotype are shown. Endogenous HTT levels were unchanged by UBQLN2 expression as measured by unpaired *t*-test. Quantification of expanded endogenous HTT levels detected by western blot and normalized to α-tubulin. (**D**) Anti-HTT immunohistochemistry (IHC) of brain sections from non-transgenic (non-Tg), HD200 mice and HD200 mice co-expressing UBQLN2. CA1: Hippocampal CA1; CTX: cortex; CB: cerebellum; STM: striatum. Scale bar = 100 µm. (**E**) Quantification of HTT nuclear inclusions in various brain regions, assessed by anti-HTT IHC. Average number of aggregates per field (six images/field per mouse) were measured for four mice from each genotype and three sections from each brain region were analyzed. Significant differences in inclusion number between HD200 single transgenic and HD200/UBQLN2 double transgenic mice were identified with unpaired *t*-test analysis, $^{*}P \leq 0.05$.

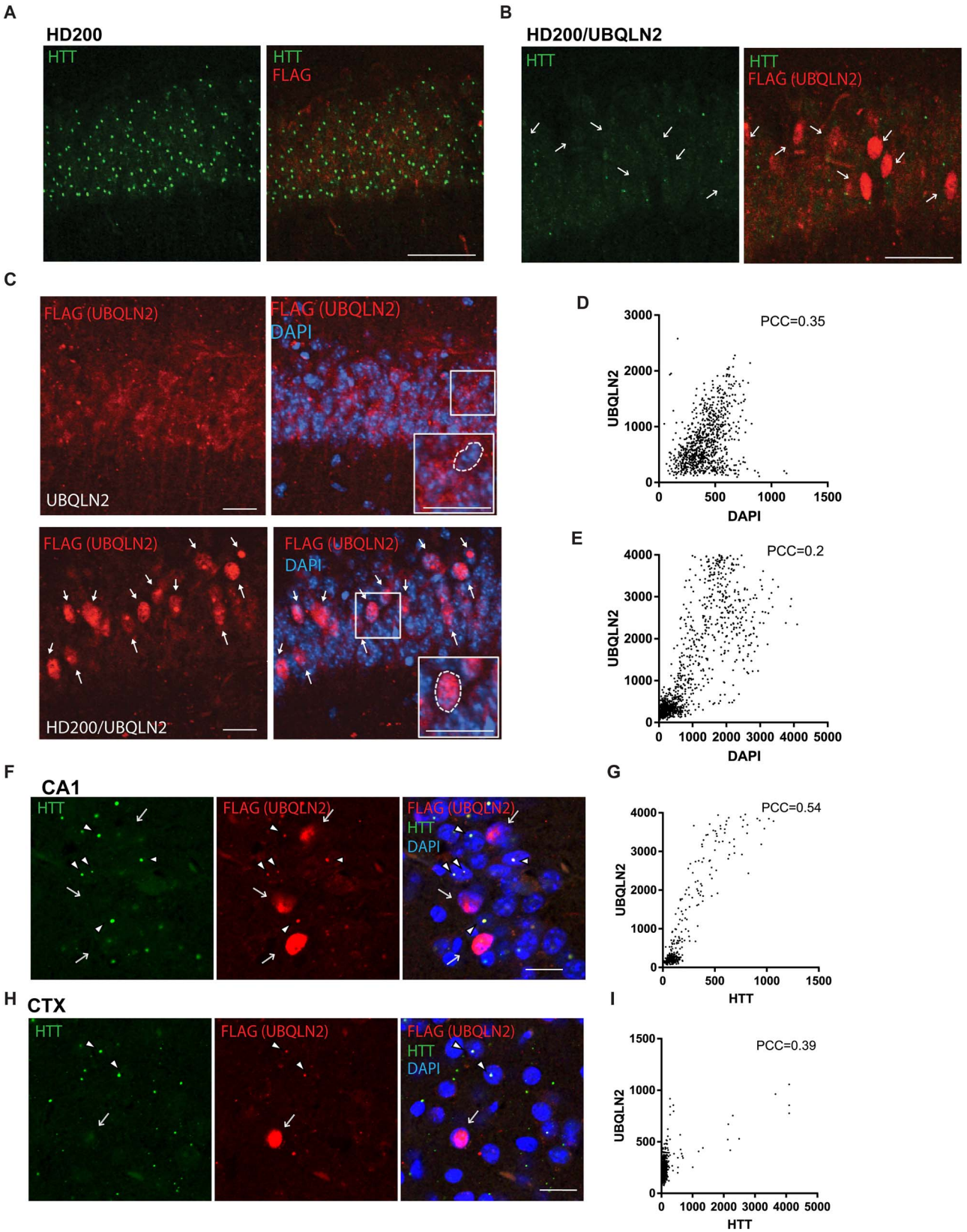

Figure 4. UBQLN2 concentrates in nuclei of neurons and co-localizes with HTT in HD200/UBQLN2 mice. (**A**) Representative immunofluorescence staining of the CA1 hippocampal region in HD200 knock-in mice and (**B**) littermate HD200 mice co-expressing FLAG-tagged UBQLN2. Sections are stained for HTT (green) and UBQLN2 (red) detected with anti-FLAG antibody. Aberrant nuclear localization of UBQLN2 is observed in a subset of cells indicated by white arrows. Note that most nuclei to which UBQLN2 localized are negative for HTT aggregates; scale bar = 50 µm. (**C**) In UBQLN2 transgenic mice, immunofluorescence of the CA1 hippocampus stained for anti-FLAG (red) and DAPI (blue) shows UBQLN2 expression mainly in the cytoplasm; scale bar = 25 µm. (**D**) In HD200/UBQLN2 mice, co-expressed UBQLN2

occurs in the cytoplasm, proteasome components are also found in the nucleus (29–31). Thus, UBQLN2 may act to promote degradation of HTT in the cytosol prior to its translocation to the nucleus or within the nucleus, as has been suggested (32). Alternatively, nuclear export may be required to degrade nuclear proteins (33). UBQLN4 has been shown to shuttle ubiquitinated proteins from the nucleus to the cytoplasmic proteasome for degradation (34), so perhaps UBQLN2 similarly promotes the export of HTT from the nucleus for degradation.

Remarkably, UBQLN2 overexpression led to an increase in cytoplasmic ATXN3 puncta, an unexpected finding given the known function of UBQLN2 in protein quality control. This result demonstrates that excess UBQLN2 is not necessarily beneficial and in some circumstances may be deleterious. While some cytoplasmic ATXN3 puncta colocalize with UBQLN2, most do not, suggesting this result does not simply reflect sequestration of ATXN3 in UBQLN2 inclusions. We favor the idea that elevated UBQLN2 in the context of ATXN3 aggregation disrupts proteasomal clearance or protein transport pathways. Our results build on earlier studies (2,35–37) that focused on links between the toxic effects of mutant UBQLN2 and impairments in protein homeostasis. Increased levels of wildtype UBQLN2 may exacerbate protein aggregation by inhibiting proteasomal degradation of certain substrates (38) or by disrupting the broader balance between protein clearance and nucleo-cytoplasmic transport (39). Previous studies on UBQLN1 support the idea that the ubiquilins may have substrate-divergent roles in the cell, in some cases reducing levels of disease proteins by facilitating proteasomal delivery (27,40) and in other cases exacerbating protein aggregation by stabilizing proteins upon binding (38,41,42). It is possible that accumulation of ATXN3 in the cytoplasm represents a failure in proteasomal clearance following translocation of ATXN3 from the nucleus mediated by UBQLN2, as has been reported for UBQLN4 (34).

Regarding the basis for the differential regulation of full-length HTT and HTT fragment by UBQLN2, perhaps UBQLN2 principally binds HTT in C-terminal regions that are missing from HTT fragment. However, UBQLN2 has been shown to interact with HTT fragment (5,15,17) and our data reveal co-localization of UBQLN2 with HTT fragment in primary neurons. Thus, we favor the hypothesis that HTT fragment forms oligomers and aggregates differently from full-length HTT, leading to differential interaction with components of protein clearance pathways, as has been reported (43), thereby decreasing the ability of UBQLN2 to facilitate degradation. Alternatively, a timing difference between full-length HTT and HTT fragment—for example, more rapid aggregation and nuclear translocation of HTT fragment—could explain the differential action of UBQLN2. HTT fragment is known to be far more aggregation-prone and to translocate to the nucleus more rapidly than full-length HTT (44). Our results demonstrating differential action of UBQLN2 on full-length versus HTT fragment are relevant to the human disease because N-terminal HTT fragments likely contribute to disease pathology in humans (45). UBQLN2 may be able to 'handle' full-length HTT under normal conditions yet lose the ability to regulate HTT in disease due, in part, to the accumulation of disease-associated HTT fragments.

A better understanding of interactions between the three brain-expressed ubiquilins (UBQLNs 1, 2 and 4) and polyglutamine disease proteins could shed light on the basis of differential UBQLN2 regulation of polyglutamine proteins. An earlier study of the interaction between UBQLN4 and another polyglutamine disease protein, SCA1 protein ATXN1, offers some insight (46). UBQLN4 was proposed to exist in two distinct conformations, one in which its UBL domain is accessible to bind the proteasome. Evidence suggested that interaction with wildtype ATXN1 prevented UBQLN4 binding to the proteasome whereas polyglutamine-expanded ATXN1 enhanced the translocation of UBQLN4 to the nucleus and allowed proteasome binding (46). Further study is required to determine if UBQLN2, which is closely homologous to UBQLN4, similarly adopts different conformations depending on the polyglutamine substrate.

Divergent post-translational modifications of disease substrates may also specify UBQLN2 action. Mutant and wildtype HTT can be differentially ubiquitinated (47) and shorter HTT fragments display distinct ubiquitin chain linkages (48). These differences in ubiquitination may in turn influence the interaction of full-length HTT and HTT fragments with UBQLN2. Though an early study of UBQLN1 suggested that ubiquilins bind K48 and K63 ubiquitin chains equally (49), recent studies of full-length ubiquilins suggest that they can differentially bind ubiquitin chains, dependent upon regions outside the UBA domain (49,50). Although ATXN3 is also ubiquitinated in disease (51,52), it can be degraded by the proteasome in a ubiquitin-independent manner (53) and may be less likely to be ubiquitinated under disease conditions than full-length HTT.

The fact that both UBQLN2 and ATXN3 regulate ubiquitin-linked protein degradation could influence their interaction. ATXN3 normally functions as a deubiquitinating enzyme whose binding to ubiquitinated substrates likely brings it in close proximity to the proteasome. Its deubiquitinase function is enhanced by ubiquitination of ATXN3 itself (51,52,54). UBQLN2 overexpression could lead to competition between UBQLN2 and ATXN3 for binding to ubiquitinated substrates and the proteasome, thus impairing proteasomal degradation of ATXN3. Supporting this possibility, another ubiquitin-proteasome shuttle factor, Rad23, inhibits ATXN3 degradation (53). Beyond its role as a deubiquitinase, ATXN3 regulates the endoplasmic reticulum-associated degradation (ERAD) pathway via shared interactors with UBQLN2, allowing both proteins to activate ERAD and regulate translocation of ubiquitinated ERAD substrates (6–8,55,56).

A limitation of this study is that differences between the two mouse models could influence the extent to which UBQLN2 does or does not affect the expressed disease protein. The HD model is a knock-in mouse expressing a CAG repeat hyperexpansion at endogenous levels, whereas the SCA3 transgenic mouse overexpresses human ATXN3 from the full human disease gene

localizes to the nuclei of many neurons (labeled with white arrows); scale bar = 25 μm. (**E**, **F**) HTT aggregates often co-localize with UBQLN2 in HD200/UBQLN2 mice. Immunofluorescence of hippocampus CA1 (E) and cortex (F) stained for anti-FLAG (red), HTT (green) and DAPI (blue) from mice co-expressing mutant HTT and UBQLN2. Arrow heads indicate puncta that are co-stained for both Flag-UBQLN2 and HTT. White arrows indicate the nuclei that are positive for Flag-UBQLN2. Note that most nuclei positive for UBQLN2 lack HTT aggregates; scale bars = 25 μm. (**G**) PCCs were calculated for the overlap of Flag-UBQLN2 and DAPI staining in neurons of HD200/UBQLN2 mice in the hippocampus (CA1) and cortex (CTX), showing that UBQLN2 frequently colocalizes with nuclear signal. By comparison, when UBQLN2 is overexpressed without HTT, UBQLN2 signal does not correlate with DAPI signal (Hippocampus: PCC = 0.007, Cortex: PCC = -0.007). (**H**) PCCs were calculated for the overlap of Flag-UBQLN2 and HTT staining in neurons of HD200/UBQLN2 mice in the hippocampus (CA1) and cortex (CTX) showing that UBQLN2 and HTT frequently colocalize.

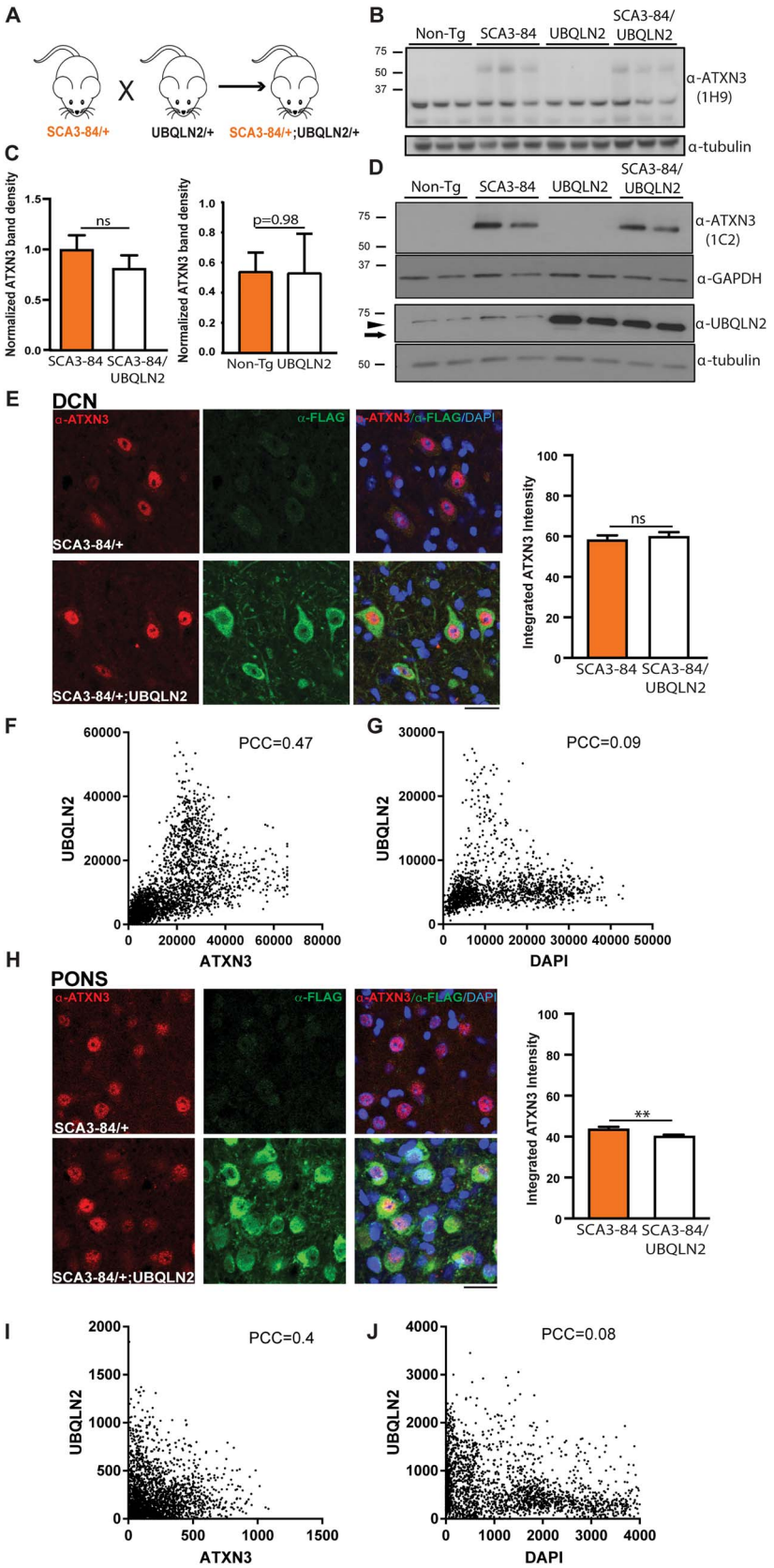

Figure 5. UBQLN2 does not reduce levels of mutant ATXN3 in whole brain lysate or intranuclear accumulation in DCN. (**A**) Breeding strategy to produce mice expressing mutant ATXN3 (SCA3–84) alone or with overexpressed UBQLN2. (**B**) Representative western blots of whole brain lysates probed with anti-ATXN3 1H9 antibody to detect mutant and endogenous murine ATXN3. Lysates from three mice of each genotype are shown. (**C**) Quantification of expanded and endogenous ATXN3 levels detected by western blot normalized to α-tubulin ($n = 5$ mice per genotype). No significant difference between SCA3–84 and SCA3–84/UBQLN2 mice or between non-Tg and UBQLN2

with an expansion within the disease range. We chose these two models because we feel they best recapitulate features of HD and SCA3, respectively. Based on the results here in cells (Fig. 1) and our prior study demonstrating that endogenous UBQLN2 interacts with HTT but not with ATXN3 (8) we believe the *in vivo* differences in UBQLN2 action against HTT and ATXN3 are not a byproduct of differences in expression between the HD and SCA3 mouse models. The fact that UBQLN2 has opposite effects on disease protein aggregation in the HD and SCA3 models (decreased in HD, increased in SCA3) also argues against an expression effect.

Taken together with previous studies observing differential localization of UBQLN2 to HTT but not ATXN3 (1,14), our results establish that UBQLN2 differentially regulates polyglutamine disease proteins. Why is UBQLN2 able to reduce the accumulation of HTT but not ATXN3? And why does UBQLN2 reduce levels of full-length mutant HTT but not HTT fragment or non-mutated HTT? These differences likely arise from the fact that (a) ATXN3 and HTT are proteins with vastly different structures and functions; (b) UBA–UBL proteins like UBQLN2 can either stabilize protein substrates or facilitate their degradation by the proteasome (46,53); and (c) when and where UBQLN2 interacts with proteins during the oligomerization/aggregation cascade may specify whether it promotes degradation. Further study is needed to understand the factors distinguishing disease proteins that UBQLN2 can 'handle' from those it cannot. Future investigations of the mechanisms by which UBQLN2 clears a subset of disease proteins through one or more protein degradation pathways may yield insights into the processes driving protein dyshomeostasis in neurodegenerative disease.

Materials and Methods

Plasmids and siRNAs

The pCMV4-FLAG-UBQLN2 plasmid (p4455 FLAG-hPLIC-2; Addgene plasmid # 8661) was a gift from Peter Howley (38). The pGW1-EGFP-HTT Exon 1 fragment 17Q and 72Q plasmids were gifts from Steven Finkbeiner (57). The full-length pTre2Hyg-FLAG-HTT 17Q and 138Q (with a phCMV-tet-responsive promoter) plasmids were gifts from Mervyn Monteiro (58). Full-length pcDNA3-myc-ATXN3 28Q and 84Q plasmids were generated as described previously (59). The pGW1-iRFP-UBQLN2 was cloned from pCMV4-FLAG-UBQLN2 into the pGW1-iRFP vector. Control empty vector plasmid for cell transfection experiments was pCMV-HA and pCMV-GFP and pGW1-iRFP were used as controls for UBQLN2 clearance experiments. Dharmacon SMARTpool siGENOME siRNA against UBQLN2 and MISSION siRNA Universal Negative Control (Sigma) were used for UBQLN2 knockdown experiments.

HEK cell transfection

Human embryonic kidney 293 (HEK-293) cells were cultured in high glucose DMEM, supplemented with 10% FBS, 10 mM Glutamine and 100 U/ml penicillin/streptomycin. Cells were transfected with either pCMV4-UBQLN2, UBQLN2 siRNA or empty vector/control siRNA in combination with GFP-HTT Exon 1 17Q or 72Q, pTre2Hyg-HTT 17Q or 138Q, ATXN3 28Q or 84Q, or pCMV-GFP using Lipofectamine-2000 according to the manufacturer's instructions. For full-length HTT experiments, cells were treated with 1 µg/ml tetracycline to induce expression. Cells used for western blot analyses were lysed in 0.5% Triton-X 100 in PBS with protease inhibitor cocktail (catalog no. 11873580001; Sigma Aldrich).

Primary neuron culture & automated microscopy

Culture and longitudinal imaging of primary rat cortical neurons has been described in detail in previous publications (9,21,60,61). Briefly, cortical neurons were dissected from embryonic day 20 rats and plated on poly-D-lysine/laminin coated 96 well plates at a density of 1×10^5 cells/well. Neurons were co-transfected with 66 ng pGW1-mApple, 66 ng pEGFP-exon1-HTT-Q17 or pEGFP-exon1-HTT-Q72, and 66 ng pGW1-iRFP or pGW1-iRFP-UBQLN2 using Lipofectamine 2000 (Invitrogen) on DIV4. A constant temperature of 37°C and 5% CO_2 was maintained during imaging by encasing the microscope in a custom-built environmental chamber. Images were acquired at 20× with an Eclipse Ti inverted microscope (Nikon) equipped with Semrock GFP, RFP and Cy5 filters, PerfectFocus, a Lambda 421 LED illumination system (Sutter Instrument) and an Andor Zyla 4.2 (+) sCMOS camera (Oxford Instruments). Automated plate movements and filter turret control were controlled via µManager. Barcode assignment for each neuron and the designation of cell-death was achieved using custom in-house software described previously (21,61,62). Quantifying the suitability of using GFP CV as a proxy for HTT puncta was performed as in previous work (9). Quantifying colocalization of UBQLN2 and HTT in puncta was carried out in CellProfiler using a custom pipeline provided for download at: https://github.com/BarmadaLab/puncta_colocalization.

Mouse models

This study was conducted in a facility approved by the American Association for the Accreditation of Laboratory Animal Care, and all experiments were performed in accordance with the National Institutes of Health 'Guide for the Care and Use of Laboratory Animals' and approved by the Institutional Animal Care and Use Committee of the University of Michigan. Mice were housed at the University of Michigan animal care facility

mice was identified (ns = not significant). (**D**) Representative western blots of whole brain lysates probed with anti-ATXN3 1C2 antibody to detect expanded ATXN3 and anti-UBQLN2 to detect UBQLN2 (arrow head labels endogenous murine UBQLN2 and arrow labels transgenic human UBQLN2). (**E**) Representative immunofluorescent image of the DCN from brain sections of SCA3–84 mice and SCA3–84/UBQLN2 mice. Quantification of nuclear accumulation of ATXN3, assessed by co-localization of ATXN3 signal (red) with DAPI (blue) was performed on images from four sections from each of three mice of both genotypes. Nuclear accumulation of mutant ATXN3 did not differ between SCA3–84 mice and SCA3–84/UBQLN2 mice (ns = not significant; mean pixel intensity for SCA3–84 mice = 58.4; $n = 1530$ nuclei; mean pixel intensity for SCA3–84/UBQLN2 mice = 60.1; $n = 1958$ nuclei). (**F**) Scatter plot of pixels positive for FLAG-UBQLN2 and ATXN3 demonstrating two largely independent populations. UBQLN2 and ATXN3 colocalize ~22% of the time in the DCN, as measured by PCC. (**G**) Scatter plot of pixels positive for FLAG-UBQLN2 and DAPI demonstrate that UBQLN2 rarely (0.8% of the time) localizes to cellular nuclei in the DCN of SCA3–84 mice. Similarly, littermate controls expressing UBQLN2 alone do not demonstrate UBQLN2 localization to nuclei (PCC = -0.09). (**H**) Representative immunofluorescent image of the pons from brain sections of SCA3–84 mice and SCA3–84/UBQLN2 mice. Nuclear accumulation of mutant ATXN3 was slightly decreased in SCA3–84/UBQLN2 mice. Quantification was performed on images from four sections from each of three mice of both genotypes. (**$P < 0.01$. Mean pixel intensity for SCA3–84 mice = 43.9; n = 2797 nuclei. Mean pixel intensity for SCA3–84/UBQLN2-WT mice = 40.4; $n = 2843$ nuclei). (**I**) Scatter plot of FLAG-UBQLN2 and ATXN3-positive pixels. UBQLN2 and ATXN3 colocalize ~16% of the time in the pons. (**J**) Scatter plot of FLAG-UBQLN2 and DAPI-positive pixels. UBQLN2 rarely (0.6% of the time) localizes to cellular nuclei in the DCN of SCA3–84 mice, similar to UBQLN2 transgenic mice not expressing ATXN3 (PCC = -0.1). Scale bar = 20 µm.

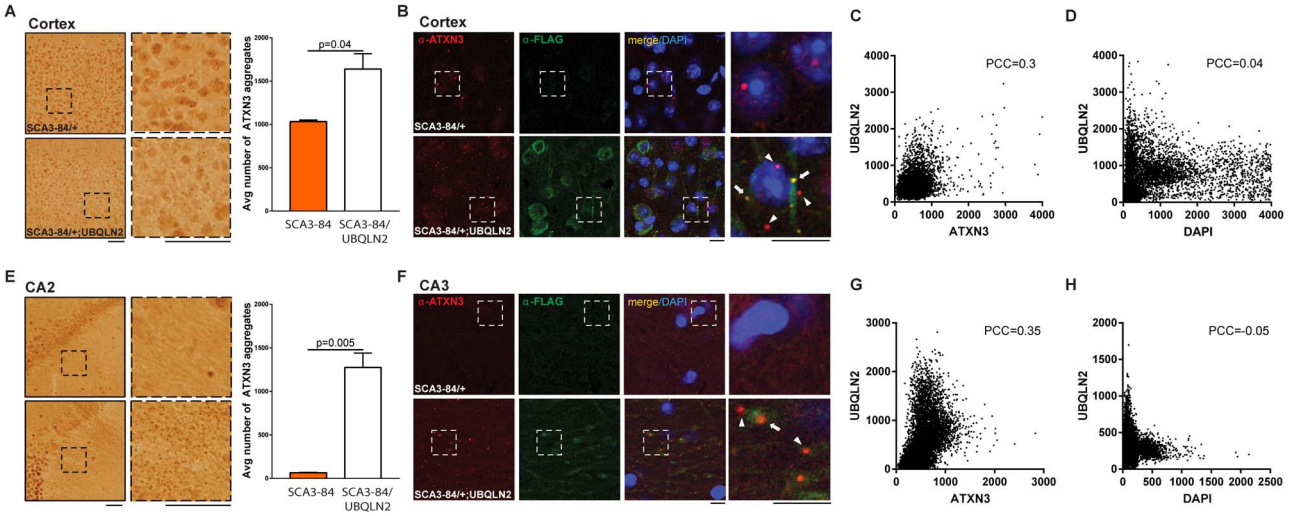

Figure 6. Overexpression of UBQLN2 induces extranuclear aggregation of mutant ATXN3 in the cortex and hippocampus of SCA3–84/UBQLN2 mice. (**A**) IHC staining of the cortex in brain sections from SCA3–84 mice show nuclear puncta of ATXN3 protein, characteristic of this disease model. SCA3–84/UBQLN2 mice also exhibit these nuclear puncta. In addition, numerous extra-nuclear puncta, not seen in the SCA3–84 mice, can be observed in SCA3–84/UBQLN2 mice. The dotted box highlighted in each image on the left corresponds to each enlarged image on the right. Quantification of ATXN3 puncta revealed significantly increased puncta in SCA3–84/UBQLN2 mice compared to SCA3–84 mice. Average number of aggregates per field were measured for four mice from each genotype and three sections from each brain region were analyzed. (**B**) Immunofluorescent staining demonstrates that extra-nuclear ATXN3 aggregates (red) in the cortex of SCA3–84/UBQLN2 mice occasionally co-localize with UBQLN2 (labeled with anti-FLAG antibody) puncta (yellow, arrows); however, many ATXN3 aggregates are not positive for UBQLN2 (arrow heads). (**C**) Scatter plot of FLAG-UBQLN2 and ATXN3-positive pixels. UBQLN2 and ATXN3 colocalize ~9% of the time in cortex, measured by PCC. (**D**) Scatter plot of FLAG-UBQLN2 and DAPI-positive pixels show that UBQLN2 rarely (0.16% of the time) localizes to cell nuclei in the cortex in SCA3–84 mice. (**E**) IHC staining of the CA2 region of the hippocampus in SCA3–84/UBQLN2 mice (bottom) shows aggregation of ATXN3 that does not occur in the SCA3–84 mice (top). Quantification of ATXN3 puncta revealed significantly increased aggregates in SCA3–84/UBQLN2 mice compared to SCA3–84 mice. Average number of aggregates per field was measured for four mice from each genotype and three sections from each brain region were analyzed. (**F**) Immunofluorescent staining shows that the ATXN3 puncta (red) in SCA3–84/UBQLN2 mice are extra-nuclear. The ATXN3 aggregates sometimes weakly co-stain for UBQLN2 (arrows) but frequently are negative for UBQLN2 (arrow heads). (**G**) Scatter plot of FLAG-UBQLN2 and ATXN3-positive pixels. UBQLN2 and ATXN3 colocalize ~12% of the time in the hippocampus. (**J**) Scatter plot of FLAG-UBQLN2-positive pixels and DAPI-positive pixels show that UBQLN2 rarely (0.2% of the time) localizes to nuclei in the hippocampus of SCA3–84 mice. Scale bars = 10 μm.

and maintained according to US Department of Agriculture standards (12 h light/dark cycle with food and water available *ad libitum*). The use of mouse models for our studies is justified based on the 3R principle by the fact that we have found UBQLN2 to behave differently with some disease proteins in animal models when compared with short time scale cell culture models. Thus, it was important to confirm that our results in cell culture translated to an *in vivo* system. Studies were adequately powered to conduct quantification of pathology by western blot and immunohistochemistry based on pilot studies in HD and SCA3 mouse models. The HD200 HD mouse model expresses murine HTT with ~200 CAG repeats (23). The SCA3-84 mouse model (YACMJD84.2Q-C57BL/6) harbors a YAC transgene that expresses a human ATXN3 gene with an expanded CAG repeat of ~84 (25,26). For genotyping of HD200 and SCA3-84 mice, DNA was extracted from mouse-tail biopsies with DNeasy Blood & Tissue Kit (Qiagen, Valencia, CA) and the DNA was sized for CAG repeat length by Laragen Inc. (Los Angeles, CA). Only mice with repeats above 185 for HD, and above 75 for SCA3-84 were utilized for our studies. To create wildtype UBQLN2 transgenic mice (9), UBQLN2 cDNA was PCR amplified using the pCMV4-FLAG-UBQLN2 plasmids as templates and cloned into the MoPrP vector (courtesy of David Borchelt, Univ. Florida) using Xho1 sites that were incorporated into the forward and reverse PCR primers. Transgenic mouse founders were generated through the UM Transgenic Animal Core. The MoPrP- UBQLN2 transgene constructs were linearized with Not1 and purified. Fertilized (C57BL/6 X SJL)F_2 mouse eggs were collected, microinjected with the linearized vector, and transferred to pseudo-pregnant recipients. When the pups were 2 weeks old, tail biopsies were taken and DNA was extracted and genotyped for the presence of the transgene. Hemizygous UBQLN2 transgenic mice were crossed to heterozygous HD-KI (Q200) and SCA3-84 SCA3 mice (23–26). Tissue from HD200 and HD200/UBQLN2 mice was collected when mice were 14–16 months old, when neuronal HTT inclusions are robustly apparent. Tissue from SCA3-84 and SCA-84/UBQLN2 mice was collected from mice at 4 months old when nuclear accumulation of mutant ATXN3 is observable.

Tissue harvesting

Animals were deeply anesthetized with ketamine/xylazine mixture and perfused transcardially with 0.1 M phosphate buffer. Brains were dissected and divided sagittally. One half was immediately placed on dry ice and stored at −80°C for biochemical studies while the other half was fixed in 4% paraformaldehyde at 4°C for 48 h, and cryoprotected in 30% sucrose in 0.1 M phosphate buffer at 4°C until saturated. Fixed hemispheres were sectioned at 40 μm sagittally through the entire hemisphere using a sledge microtome (SM200R; Leica Biosystems). Free-floating sections were stored at −20°C for immunostaining.

Western blot analysis

Cell lysates were sonicated for 5 min in chilled water, centrifuged at 10000 rcf for 10 min at 4°C and supernatants were collected. For whole brain lysates used to quantify levels of endogenous ATXN3 or HTT in UBQLN2 transgenic mice, mouse

brain samples were homogenized in RIPA buffer with protease inhibitor cocktail (catalog no. 11873580001; Sigma Aldrich), using a 1:3 dilution of tissue: RIPA (w/v). Samples were centrifuged at 16000 rcf for 30 min at 4°C. Supernatants were aliquoted, snap-frozen and stored at −80°C until use. For detection of HTT or ATXN3 in HD200 and HD200/UBQLN2 or SCA3-84 and SCA3-84/UBQLN2 brains, lysates from brain tissue were prepared in RIPA buffer (cat #R0278, Sigma) with protease inhibitors (Roche), PMSF and PhosphoStop (Roche). Brain tissue was homogenized in a Potter homogenizer followed by incubation on ice for 1 h to complete lysis. Samples were sonicated, centrifuged (13000 rpm for 30 min) and the supernatants were removed. Samples were prepared in 1× Laemmli sample buffer with DTT, heated at 100°C for 5 min and centrifuged for 5 min at 13000 rpm. Protein concentration was measured using a BCA assay (cat#23227, ThermoScientific).

Cell lysates containing 10 µg of total protein were loaded (without boiling) on precast NuPAGE 4–12% Bis-Tris gels (Invitrogen) for SDS-PAGE analysis. Brain extracts containing 25 µg of total protein were loaded after boiling on precast Novex NuPAGE 3–8% Tris-Acetate gels, 1.5 mm, 15 well (cat#EA03785BOX, LifeTechnogies) for SDS-PAGE analysis. Gels were run in NuPage Tris-Acetate SDS running buffer 20× (cat#LA0041, LifeTechnologies) at 150 V at room temperature (RT) and subsequently transferred either onto nitrocellulose membranes, 0.45 µm, at 110 V for 1 h at 4°C or PVDF membrane, 0.45 µm, at 0.35A for 3 h at 4°C. Membranes were blocked for 1 h at RT with either 5 or 10% nonfat dry milk in TBS-T buffer. Membranes were then probed overnight at 4°C in anti-Ubiquilin-2 (Novus Biologicals; 1:2000), anti-HTT, clone mEM48 (Millipore; 1:500), anti-FLAG, clone M2 (Sigma, 1:1000), anti-ATXN3, clone 1H9 (Millipore, cat# MAB5360, 1:1000), anti-GFP, clone 11E5 (ThermoFisher; 1:1000), anti-HTT, clone 1HU-4C8 (Millipore Sigma; 1:500), anti-1C2 for detection of polyQ-expanded HTT (Millipore, cat# MAB1574; 1:5000), anti-GAPDH (Millipore; 1:5000) or anti-α-tubulin (Cell Signaling, cat# 2144; 1:1000) diluted in 5% nonfat dry milk. HRP-conjugated goat anti-rabbit IgG or goat anti-mouse IgG (1:5000) were used for detection as appropriate. ECL (Pierce) was used to visualize bands developed either by film (Figs 1, 3B, and 5) or using the Syngene G:Box imaging system (Fig. 3C), which were normalized to corresponding GAPDH or α-tubulin levels using low exposure images within the linear range of ECL. All quantification of immunoblots was performed by densitometric analysis of averaged western blots completed in triplicate using ImageJ software (National Institutes of Health).

Immunohistochemistry

Immunohistochemistry was performed as described previously (24,63). Briefly, free-floating sections were labeled with goat anti-N-terminal HTT (1:250; Santa Cruz Biotechnology). Immunostaining was performed using the Vectastain Elite Kit (Vector Laboratories, Burlingame, CA). Sections were developed in ImmPACT DAB (Vector Laboratories), mounted on Superfrost slides (Fisher Scientific, Pittsburgh, PA) and air dried after dehydration with graded ethanol and xylene. Coverslips were affixed with DPX (Electron Microscopy Sciences, Hatfield PA, USA). All sections were imaged with an Olympus BX51 microscope (Olympus, Center Valley, PA). Quantification of HTT and ATXN3-positive inclusions was performed using ImageJ software. The average number of inclusions was determined by analyzing four fields of view per brain region from each of four animals.

Immunofluorescence

Brain sections were subjected to a basic antigen retrieval, washed, blocked and incubated overnight at 4°C in primary antibody supplemented with 0.025% Triton X-100, 0.5% BSA, and 5% serum from the host line for secondary antibodies (donkey or goat). Primary antibodies used in these studies included the following: rabbit anti-FLAG (1:1000, Sigma) 1:1000, anti-ATXN3, clone 1H9 (1:1000, Sigma) and goat anti-N-terminal HTT (1:250; Santa Cruz Biotechnology). Primary incubated sections were then washed and incubated with the corresponding secondary Alexa Fluor 488 or 568 antibodies (1:1000; Invitrogen). All sections were stained with DAPI (Sigma) for 15 min at RT, mounted with Prolong Gold Antifade Reagent (Invitrogen) and imaged using an IX71 Olympus inverted microscope or Olympus confocal microscope. Quantification of nuclear ATXN3 was performed using cell profiler, an open source cell imaging analysis software https://cellprofiler.org (64). Nuclear accumulation of ATXN3 was quantified by measuring the degree of colocalization of immuno-labeled ATXN3 with the DAPI signal. Colocalization analyses were performed on thresholded images using the EZColocalization plugin in ImageJ. Representative pixel scatter plots are displayed for colocalization analyses, as well as the average Pearson's correlation coefficient (PCC) for all analyzed images. Colocalization analyses were completed using four fields of view per brain region from each of four animals.

Experimental design and statistical analysis

All western blot analyses were repeated in triplicate and statistical analyses utilized means from the three replicates. The accepted level of significance for all analyses was $P \leq 0.05$. All analyses comparing two groups were analyzed using student's *t*-test and comparisons between three or more groups were completed by one-way ANOVA and the Bonferroni *post-hoc* test. Data are expressed as means ± SEM. P-values for overall ANOVAs are displayed in analyses that did not show a significant difference and individual *post-hoc* comparison P-values are displayed for significant ANOVAs. Data were analyzed in Statview (SAS Institute), with the exception of survival data in Figure 2, which were analyzed using the survival package in R, and immunohistochemistry and immunofluorescence data, which were assessed using GraphPad Prism.

Supplementary Material

Supplementary Material is available at *HMG* online.

Acknowledgements

We thank Peter Howley, Steven Finkbeiner and Mervyn Monteiro for providing constructs, and Paulson lab members for their helpful suggestions. This work was supported by NIH 9R01NS096785-06, 1P30AG053760-01, F32-AG059362-01, T32-NS007222-36, the Alzheimer's Association and The Amyotrophic Lateral Sclerosis Foundation.

Conflict of Interest statement. None declared.

References

1. Mori, F., Tanji, K., Odagiri, S., Toyoshima, Y., Yoshida, M., Ikeda, T., Sasaki, H., Kakita, A., Takahashi, H. and Wakabayashi, K. (2012) Ubiquilin immunoreactivity in cytoplasmic and

nuclear inclusions in synucleinopathies, polyglutamine diseases and intranuclear inclusion body disease. *Acta Neuropathol.*, **124**, 149–151.
2. Deng, H.-X., Chen, W., Hong, S.-T., Boycott, K.M., Gorrie, G.H., Siddique, N., Yang, Y., Fecto, F., Shi, Y., Zhai, H. *et al.* (2011) Mutations in UBQLN2 cause dominant X-linked juvenile and adult onset ALS and ALS/dementia. *Nature*, **477**, 211–215.
3. Elsasser, S., Gali, R.R., Schwickart, M., Larsen, C.N., Leggett, D.S., Muller, B., Feng, M.T., Tubing, F., Dittmar, G.A.G. and Finley, D. (2002) Proteasome subunit Rpn1 binds ubiquitin-like protein domains. *Nat. Cell Biol.*, **4**, 725–730.
4. Rao, H. and Sastry, A. (2002) Recognition of specific ubiquitin conjugates is important for the Proteolytic functions of the ubiquitin-associated domain proteins Dsk2 and Rad23. *J. Biol. Chem.*, **277**, 11691–11695.
5. Chuang, K.-H., Liang, F., Higgins, R. and Wang, Y. (2016) Ubiquilin/Dsk2 promotes inclusion body formation and vacuole (lysosome)-mediated disposal of mutated huntingtin. *Mol. Biol. Cell*, **27**, 2025–2036.
6. Lim, P.J., Danner, R., Liang, J., Doong, H., Harman, C., Srinivasan, D., Rothenberg, C., Wang, H., Ye, Y., Fang, S. and Monteiro, M.J. (2009) Ubiquilin and p97/VCP bind erasin, forming a complex involved in ERAD. *J. Cell Biol.*, **187**, 201–217.
7. Halloran, M., Ragagnin, A.M.G., Vidal, M., Parakh, S., Yang, S., Heng, B., Grima, N., Shahheydari, H., Soo, K.-Y., Blair, I. *et al.* (2019) Amyotrophic lateral sclerosis-linked UBQLN2 mutants inhibit endoplasmic reticulum to Golgi transport, leading to Golgi fragmentation and ER stress. *Cell. Mol. Life Sci.*, in press. doi: 10.1007/s00018-019-03394-w.
8. Xia, Y., Yan, L.H., Huang, B., Liu, M., Liu, X. and Huang, C. (2014) Pathogenic mutation of UBQLN2 impairs its interaction with UBXD8 and disrupts endoplasmic reticulum-associated protein degradation. *J. Neurochem.*, **129**, 99–106.
9. Sharkey, L.M., Safren, N., Pithadia, A.S., Gerson, J.E., Dulchavsky, M., Fischer, S., Patel, R., Lantis, G., Ashraf, N., Kim, J.H. *et al.* (2018) Mutant UBQLN2 promotes toxicity by modulating intrinsic self-assembly. *Proc. Natl. Acad. Sci. USA.*, **115**, E10495–E10504.
10. Dao, T.P., Kolaitis, R.-M., Kim, H.J., O'Donovan, K., Martyniak, B., Colicino, E., Hehnly, H., Taylor, J.P. and Castañeda, C.A. (2018) Ubiquitin modulates liquid-liquid phase separation of UBQLN2 via disruption of multivalent interactions. *Mol. Cell*, **69**, 965–978.e966.
11. Scotter, E.L., Smyth, L., Bailey, J.A.W.T., Wong, C.-H., de Majo, M., Vance, C.A., Synek, B.J., Turner, C., Pereira, J., Charleston, A. *et al.* (2017) C9ORF72 and UBQLN2 mutations are causes of amyotrophic lateral sclerosis in New Zealand: a genetic and pathologic study using banked human brain tissue. *Neurobiol. Aging*, **49**, 214.e211–214.e215.
12. Fahed, A.C., McDonough, B., Gouvion, C.M., Newell, K.L., Dure, L.S., Bebin, M., Bick, A.G., Seidman, J.G., Harter, D.H. and Seidman, C.E. (2014) UBQLN2 mutation causing heterogeneous X-linked dominant Neurodegeneration. *Ann. Neurol.*, **75**, 793–798.
13. Williams, K.L., Warraich, S.T., Yang, S., Solski, J.A., Fernando, R., Rouleau, G.A., Nicholson, G.A. and Blair, I.P. (2012) UBQLN2/ubiquilin 2 mutation and pathology in familial amyotrophic lateral sclerosis. *Neurobiol. Aging*, **33**, 2527.e2523–2527.e2510.
14. Zeng, L., Wang, B., Merillat, S.A., Minakawa, E., Perkins, M.D., Ramani, B., Tallaksen-Greene, S.J., do Carmo Costa, M., Albin, R.L. and Paulson, H.L. (2015) Differential recruitment of UBQLN2 to nuclear inclusions in the polyglutamine diseases HD and SCA3. *Neurobiol. Dis.*, **82**, 281–288.
15. Safren, N., Chang, L., Dziki, K.M. and Monteiro, M.J. (2015) Signature changes in ubiquilin expression in the R6/2 mouse model of Huntington's disease. *Brain Res.*, **1597**, 37–46.
16. Rutherford, N.J., Lewis, J., Clippinger, A.K., Thomas, M.A., Adamson, J., Cruz, P.E., Cannon, A., Xu, G., Golde, T.E., Shaw, G. *et al.* (2013) Unbiased screen reveals ubiquilin-1 and -2 highly associated with huntingtin inclusions. *Brain Res.*, **1524**, 62–73.
17. Hjerpe, R., Bett, J.S., Keuss, M.J., Solovyova, A., McWilliams, T.G., Johnson, C., Sahu, I., Varghese, J., Wood, N., Wightman, M. *et al.* (2016) UBQLN2 mediates autophagy-independent protein aggregate clearance by the proteasome. *Cell*, **166**, 935–949.
18. Seidel, K., Siswanto, S., Fredrich, M., Bouzrou, M., den Dunnen, W.F.A., Özerden, I., Korf, H.-W., Melegh, B., de Vries, J.J., Brunt, E.R. *et al.* (2017) On the distribution of intranuclear and cytoplasmic aggregates in the brainstem of patients with spinocerebellar ataxia type 2 and 3. *Brain Pathol.*, **27**, 345–355.
19. Wheeler, V.C., White, J.K., Gutekunst, C.-A., Vrbanac, V., Weaver, M., Li, X.-J., Li, S.-H., Yi, H., Vonsattel, J.-P., Gusella, J.F. *et al.* (2000) Long glutamine tracts cause nuclear localization of a novel form of huntingtin in medium spiny striatal neurons in HdhQ92 and HdhQ111 knock-in mice. *Hum. Mol. Genet.*, **9**, 503–513.
20. Paulson, H.L., Perez, M.K., Trottier, Y., Trojanowski, J.Q., Subramony, S.H., Das, S.S., Vig, P., Mandel, J.L., Fischbeck, K.H. and Pittman, R.N. (1997) Intranuclear inclusions of expanded polyglutamine protein in spinocerebellar ataxia type 3. *Neuron*, **19**, 333–344.
21. Weskamp, K., Safren, N., Miguez, R. and Barmada, S. (2019) Monitoring neuronal survival via longitudinal fluorescence microscopy. *J. Vis. Exp.*, in press. doi: 10.3791/59036.
22. Ramdzan, Y.M., Polling, S., Chia, C.P.Z., Ng, I.H.W., Ormsby, A.R., Croft, N.P., Purcell, A.W., Bogoyevitch, M.A., Ng, D.C.H., Gleeson, P.A. and Hatters, D.M. (2012) Tracking protein aggregation and mislocalization in cells with flow cytometry. *Nat. Methods*, **9**, 467–470.
23. Heng, M.Y., Duong, D.K., Albin, R.L., Tallaksen-Greene, S.J., Hunter, J.M., Lesort, M.J., Osmand, A., Paulson, H.L. and Detloff, P.J. (2010) Early autophagic response in a novel knock-in model of Huntington disease. *Hum. Mol. Genet.*, **19**, 3702–3720.
24. Zeng, L., Tallaksen-Greene, S.J., Wang, B., Albin, R.L. and Paulson, H.L. (2013) The de-ubiquitinating enzyme ataxin-3 does not modulate disease progression in a knock-in mouse model of Huntington disease. *J. Huntington's Dis.*, **2**, 201–215.
25. Cemal, C.K., Carroll, C.J., Lawrence, L., Lowrie, M.B., Ruddle, P., Al-Mahdawi, S., King, R.H.M., Pook, M.A., Huxley, C. and Chamberlain, S. (2002) YAC transgenic mice carrying pathological alleles of the MJD1 locus exhibit a mild and slowly progressive cerebellar deficit. *Hum. Mol. Genet.*, **11**, 1075–1094.
26. Shakkottai, V.G., do Carmo Costa, M., Dell'Orco, J.M., Sankaranarayanan, A., Wulff, H. and Paulson, H.L. (2011) Early changes in cerebellar physiology accompany motor dysfunction in the polyglutamine disease spinocerebellar ataxia type 3. *J. Neurosci.*, **31**, 13002–13014.
27. Safren, N., El Ayadi, A., Chang, L., Terrillion, C.E., Gould, T.D., Boehning, D.F. and Monteiro, M.J. (2014) Ubiquilin-1 overexpression increases the lifespan and delays accumulation of Huntingtin aggregates in the R6/2 mouse model of Huntington's disease. *PLoS One*, **9**, e87513.

28. Massey, T.H. and Jones, L. (2018) The central role of DNA damage and repair in CAG repeat diseases. *Dis. Model. Mech.*, **11**, dmm031930.
29. Savulescu, A.F., Rotem, A. and Harel, A. (2011) Proteasomes crossing the nuclear border. *Nucleus*, **2**, 258–263.
30. Krüger, E., Kloetzel, P.-M. and Enenkel, C. (2001) 20S proteasome biogenesis. *Biochimie*, **83**, 289–293.
31. Enenkel, C., Lehmann, A. and Kloetzel, P.M. (1998) Subcellular distribution of proteasomes implicates a major location of protein degradation in the nuclear envelope-ER network in yeast. *EMBO J.*, **17**, 6144–6154.
32. Samant, R.S., Livingston, C.M., Sontag, E.M. and Frydman, J. (2018) Distinct proteostasis circuits cooperate in nuclear and cytoplasmic protein quality control. *Nature*, **563**, 407–411.
33. Chen, L. and Madura, K. (2014) Degradation of specific nuclear proteins occurs in the cytoplasm in saccharomyces cerevisiae. *Genetics*, **197**, 193–197.
34. Hirayama, S., Sugihara, M., Morito, D., Iemura, S.-I., Natsume, T., Murata, S. and Nagata, K. (2018) Nuclear export of ubiquitinated proteins via the UBIN-POST system. *Proc. Natl. Acad. Sci. USA.*, **115**, E4199–E4208.
35. Chen, T., Huang, B., Shi, X., Gao, L. and Huang, C. (2018) Mutant UBQLN2(P497H) in motor neurons leads to ALS-like phenotypes and defective autophagy in rats. *Acta Neuropathol. Commun.*, **6**, 122.
36. Osaka, M., Ito, D. and Suzuki, N. (2016) Disturbance of proteasomal and autophagic protein degradation pathways by amyotrophic lateral sclerosis-linked mutations in ubiquilin 2. *Biochem. Biophys. Res. Commun.*, **472**, 324–331.
37. Chang, L. and Monteiro, M.J. (2015) Defective proteasome delivery of Polyubiquitinated proteins by Ubiquilin-2 proteins containing ALS mutations. *PLoS One*, **10**, e0130162.
38. Kleijnen, M.F., Shih, A.H., Zhou, P., Kumar, S., Soccio, R.E., Kedersha, N.L., Gill, G. and Howley, P.M. (2000) The hPLIC proteins may provide a link between the ubiquitination machinery and the proteasome. *Mol. Cell*, **6**, 409–419.
39. Picher-Martel, V., Dutta, K., Phaneuf, D., Sobue, G. and Julien, J.-P. (2015) Ubiquilin-2 drives NF-κB activity and cytosolic TDP-43 aggregation in neuronal cells. *Mol. Brain*, **8**, 71.
40. Adegoke, O.O., Qiao, F., Liu, Y., Longley, K., Feng, S. and Wang, H. (2017) Overexpression of Ubiquilin-1 alleviates Alzheimer's disease-caused cognitive and motor deficits and reduces amyloid-β accumulation in mice. *J. Alzheimers Dis.*, **59**, 575–590.
41. Massey, L.K., Mah, A.L., Ford, D.L., Miller, J., Liang, J., Doong, H. and Monteiro, M.J. (2004) Overexpression of ubiquilin decreases ubiquitination and degradation of presenilin proteins. *J. Alzheimers Dis.*, **6**, 79–92.
42. Saliba, R.S., Pangalos, M. and Moss, S.J. (2008) The ubiquitin-like protein Plic-1 enhances the membrane insertion of GABAA receptors by increasing their stability within the endoplasmic reticulum. *J. Biol. Chem.*, **283**, 18538–18544.
43. Chai, Y., Wu, L., Griffin, J.D. and Paulson, H.L. (2001) The role of protein composition in specifying nuclear inclusion formation in polyglutamine disease. *J. Biol. Chem.*, **276**, 44889–44897.
44. Landles, C., Sathasivam, K., Weiss, A., Woodman, B., Moffitt, H., Finkbeiner, S., Sun, B., Gafni, J., Ellerby, L.M., Trottier, Y. *et al.* (2010) Proteolysis of mutant huntingtin produces an exon 1 fragment that accumulates as an aggregated protein in neuronal nuclei in Huntington disease. *J. Biol. Chem.*, **285**, 8808–8823.
45. Kim, Y.J., Yi, Y., Sapp, E., Wang, Y., Cuiffo, B., Kegel, K.B., Qin, Z.H., Aronin, N. and DiFiglia, M. (2001) Caspase 3-cleaved N-terminal fragments of wild-type and mutant huntingtin are present in normal and Huntington's disease brains, associate with membranes, and undergo calpain-dependent proteolysis. *Proc. Natl. Acad. Sci. USA.*, **98**, 12784–12789.
46. Riley, B.E., Xu, Y., Zoghbi, H.Y. and Orr, H.T. (2004) The effects of the polyglutamine repeat protein Ataxin-1 on the UbL-UBA protein A1Up. *J. Biol. Chem.*, **279**, 42290–42301.
47. Sap, K.A., Guler, A.T., Bezstarosti, K., Bury, A.E., Juenemann, K., Demmers, J.A.A. and Reits, E.A. (2019) Global proteome and ubiquitinome changes in the soluble and insoluble fractions of Q175 Huntington mice brains. *Mol. Cell. Proteomics*, **18**, 1705–1720.
48. Bhat, K.P., Yan, S., Wang, C.-E., Li, S. and Li, X.-J. (2014) Differential ubiquitination and degradation of huntingtin fragments modulated by ubiquitin-protein ligase E3A. *Proc. Natl. Acad. Sci. USA.*, **111**, 5706–5711.
49. Zhang, D., Raasi, S. and Fushman, D. (2008) Affinity makes the difference: nonselective interaction of the UBA domain of Ubiquilin-1 with monomeric ubiquitin and Polyubiquitin chains. *J. Mol. Biol.*, **377**, 162–180.
50. Harman, C.A. and Monteiro, M.J. (2019) The specificity of ubiquitin binding to ubiquilin-1 is regulated by sequences besides its UBA domain. *Biochim. Biophys. Acta*, **1863**, 1568–1574.
51. Todi, S.V., Winborn, B.J., Scaglione, K.M., Blount, J.R., Travis, S.M. and Paulson, H.L. (2009) Ubiquitination directly enhances activity of the deubiquitinating enzyme ataxin-3. *EMBO J.*, **28**, 372–382.
52. Tsou, W.-L., Burr, A.A., Ouyang, M., Blount, J.R., Scaglione, K.M. and Todi, S.V. (2013) Ubiquitination regulates the neuroprotective function of the deubiquitinase ataxin-3 in vivo. *J. Biol. Chem.*, **288**, 34460–34469.
53. Blount, J.R., Tsou, W.-L., Ristic, G., Burr, A.A., Ouyang, M., Galante, H., Scaglione, K.M. and Todi, S.V. (2014) Ubiquitin-binding site 2 of ataxin-3 prevents its proteasomal degradation by interacting with Rad23. *Nat. Commun.*, **5**, 4638.
54. Todi, S.V., Scaglione, K.M., Blount, J.R., Basrur, V., Conlon, K.P., Pastore, A., Elenitoba-Johnson, K. and Paulson, H.L. (2010) Activity and cellular functions of the Deubiquitinating enzyme and Polyglutamine disease protein Ataxin-3 are regulated by Ubiquitination at lysine 117. *J. Biol. Chem.*, **285**, 39303–39313.
55. Wang, Q., Li, L. and Ye, Y. (2006) Regulation of retrotranslocation by p97-associated deubiquitinating enzyme ataxin-3. *J. Cell Biol.*, **174**, 963–971.
56. Zhong, X. and Pittman, R.N. (2006) Ataxin-3 binds VCP/p97 and regulates retrotranslocation of ERAD substrates. *Hum. Mol. Genet.*, **15**, 2409–2420.
57. Miller, J., Arrasate, M., Shaby, B.A., Mitra, S., Masliah, E. and Finkbeiner, S. (2010) Quantitative relationships between Huntingtin levels, polyglutamine length, inclusion body formation, and neuronal death provide novel insight into Huntington's disease molecular pathogenesis. *J. Neurosci.*, **30**, 10541–10550.
58. Yang, H., Zhong, X., Ballar, P., Luo, S., Shen, Y., Rubinsztein, D.C., Monteiro, M.J. and Fang, S. (2007) Ubiquitin ligase Hrd1 enhances the degradation and suppresses the toxicity of polyglutamine-expanded huntingtin. *Exp. Cell Res.*, **313**, 538–550.

59. Chai, Y., Koppenhafer, S.L., Bonini, N.M. and Paulson, H.L. (1999) Analysis of the role of heat shock protein (Hsp) molecular chaperones in Polyglutamine disease. *J. Neurosci.*, **19**, 10338–10347.
60. Flores, B.N., Li, X., Malik, A.M., Martinez, J., Beg, A.A. and Barmada, S.J. (2019) An Intramolecular salt bridge linking TDP43 RNA binding, protein stability, and TDP43-dependent Neurodegeneration. *Cell Rep.*, **27**, 1133–1150.e8.
61. Malik, A.M., Miguez, R.A., Li, X., Ho, Y.-S., Feldman, E.L. and Barmada, S.J. (2018) Matrin 3-dependent neurotoxicity is modified by nucleic acid binding and nucleocytoplasmic localization. *elife*, **7**, e35977.
62. Arrasate, M. and Finkbeiner, S. (2005) Automated microscope system for determining factors that predict neuronal fate. *Proc. Natl. Acad. Sci. USA.*, **102**, 3840–3845.
63. Costa, M.D.C., Luna-Cancalon, K., Fischer, S., Ashraf, N.S., Ouyang, M., Dharia, R.M., Martin-Fishman, L., Yang, Y., Shakkottai, V.G., Davidson, B.L. *et al.* (2013) Toward RNAi therapy for the polyglutamine disease Machado-Joseph disease. *Mol. Ther.*, **21**, 1898–1908.
64. McQuin, C., Goodman, A., Chernyshev, V., Kamentsky, L., Cimini, B.A., Karhohs, K.W., Doan, M., Ding, L., Rafelski, S.M., Thirstrup, D. *et al.* (2018) CellProfiler 3.0: next-generation image processing for biology. *PLoS Biol.*, **16**, e2005970.